



Glycerol valorization by etherification to polyglycerols by using metal oxides derived from MgFe hydrotalcites

P. Guerrero-Urbaneja, C. García-Sancho, R. Moreno-Tost*, J. Mérida-Robles,
J. Santamaría-González, A. Jiménez-López, P. Maireles-Torres

Departamento de Química Inorgánica, Mineralogía y Cristalografía (Unidad Asociada al ICP-CSIC), Facultad de Ciencias, Universidad de Málaga,
Campus de Teatinos s/n, 29071 Málaga, Spain

ARTICLE INFO

Article history:

Received 8 July 2013
Received in revised form 24 October 2013
Accepted 25 October 2013
Available online 5 November 2013

Keywords:

Layered double hydroxide
Iron
Glycerol
Etherification
Polyglycerol

ABSTRACT

This work investigates the use of MgFe mixed oxides, derived from layered double hydroxides (LDH) with Mg/Fe molar ratio ranging from 1 to 4, as base catalysts for the etherification of glycerol. LDH precursors and catalysts were characterized by XRD, XPS, CO₂-TPD, NH₃-TPD, N₂ adsorption and DTA-TG analysis. The MgFe mixed oxides exhibit excellent textural properties, with specific surface areas close to 200 m² g⁻¹ and average pore diameters in the mesoporous range. This family of catalysts has shown to be active in the formation of polyglycerols from glycerol without solvent, at 220 °C, in a batch reactor. The highest conversion (41%) is found for the MgFeO₄ catalyst prepared with a Mg/Fe molar ratio of 4, whereas full selectivity to diglycerols is only reached for the MgFeO₁ catalyst. Only diglycerols (DGs) and triglycerols (TGs) have been detected after 24 h of reaction.

© 2013 Elsevier B.V. All rights reserved.

1. Introduction

Biodiesel and bioethanol are the two most important biofuels successfully supplied in the transportation sector. In Europe, the production of biodiesel is increased from 4.1 MTm in 2006 up to 9.6 MTm in 2010 [1]. Biodiesel is a mixture of long-chain alkyl esters produced by transesterification of vegetable oils with short-chain alcohols, such as methanol or ethanol. Glycerol is generated as by-product in this transesterification process (roughly 10 wt%), giving rise to a stock of glycerol which requires to be efficiently valorized in order to obtain a more sustainable biodiesel production. In this sense, glycerol has been turned into an interesting starting raw material for other chemical products. In recent years, several reviews [2–4], dealing with the potential uses of glycerol as starting compound for many industrial applications, have been published. An interesting valorization alternative is the glycerol oligomerisation [5,6], because these oligomers are already used in cosmetics and, as additives, in nutrition or lubricants. The condensation of two glycerol molecules yields diglycerol, the simplest polyglycerol, which can be linear, branched or cyclic depending on if the condensation takes place between primary or secondary hydroxyls, or an intramolecular condensation is involved [5]. On the other hand, the condensation of glycerol can progress yielding tri-, tetra- and

higher polyglycerols. This etherification process is carried out in the presence of basic homogeneous catalysts, mainly alkaline carbonates or hydroxides. Thus, Ayoub et al. [7] have demonstrated that LiOH exhibits an excellent catalytic performance, reaching full glycerol conversion, with a selectivity of 33% towards diglycerol, after 6 h of reaction. Clacens et al. [8–10] have shown, that concerning the selectivity, the best results were obtained over mesoporous solids modified by exchanged or impregnation with Cs. On the other hand, Ruppert et al. [11] studied the use of alkaline earth metal oxides at lower temperature (220 °C) and compared the catalytic results with homogeneous sodium carbonate. Thus, they found that glycerol conversion enhanced with increasing catalyst basicity: MgO < CaO < SrO < BaO. The best selectivity values for (di- + tri-) glycerol (>90% at 60% conversion) were obtained over CaO, SrO, and BaO, with no substantial acrolein formation. However, alkaline earth oxides suffer from instability toward ambient water and carbon dioxide, giving rise to less basic species, thus requiring very high activation temperatures. Gholami et al. [12], evaluating the activity of Ca:Al:La composites, concluded that the most suitable La:Ca molar ratio was 1:2.7, reaching 91% glycerol conversion and a selectivity towards diglycerol of 53%. Recently, we reported the catalytic performance of MgAl mixed oxides derived from the corresponding hydrotalcite in the etherification of glycerol [13], being the most active catalyst the mixed oxide derived from the hydrotalcite prepared by the coprecipitation method using Na₂CO₃/NaOH as precipitant agent. This catalyst yielded a maximum conversion of 51% and a diglycerol selectivity of 85%. Razealy-Anuar et al.

* Corresponding author. Tel.: +34 952132021; fax: +34 952131870.

E-mail address: rmtost@uma.es (R. Moreno-Tost).



[14] described the activity of MgAl hydrotalcite synthesized by the combustion method. This catalyst reached the highest glycerol conversion in 16 h (77.7% glycerol conversion) and when the glucose was used as fuel and calcined at 650 °C.

Among basic solids, mixed metal oxides derived from layered double hydroxides (LDHs) seem to be very promising for practical applications due to the easiness of synthesis and handling [15]. These solids are represented by the general formula $[M^{2+}_{1-x}M^{3+}_x(OH)_2]A^{n-}_{x/n}\cdot mH_2O$ [16], where M^{2+} and M^{3+} are di- and trivalent metal cations, including cations such as Mg^{2+} , Fe^{2+} , Ni^{2+} , Cu^{2+} , Co^{2+} , Mn^{2+} , Zn^{2+} or Cd^{2+} and Al^{3+} , Cr^{3+} , Ga^{3+} or Fe^{3+} , respectively. A^{n-} is an interlayer anion and x is the $[M^{3+}] / ([M^{2+}] + [M^{3+}])$ molar fraction. Their structure consists of brucite-type layers where M^{2+} cations are partially replaced with M^{3+} cations, inducing a net positive charge, which is compensated by anions situated in the interlayer region (e.g., CO_3^{2-} , SO_4^{2-} , NO_3^- , $C1^-$, OH^-) together with water molecules. An important feature of this family of solids is that their basicity, interlayer distance and crystallites morphology can be tailored by adjusting the nature of the cations, the metal ratio in the brucite-like layers and the interlayer anionic species [16]. Both the basic properties of hydrotalcite-like materials and the existence of well-dispersed mixed oxides upon thermal decomposition are key aspects for successful application in catalysis.

Hydrotalcites, wherein Fe^{3+} ion partially substitutes Mg^{2+} , are among the most studied, as catalyst precursors. MgFe mixed oxides generated after thermal treatment, usually at 450 °C, have demonstrated to be excellent sorbent for phosphate [17] or perchlorate ions [18]. Moreover, these solids show acid-base properties [19], participating in dehydrogenation reactions over basic sites and dehydration reactions over acidic ones [18,20]. Thus, these mixed oxides have found applications in dehydrogenation of ethylbenzene to styrene [21,22], alkylation of *m*-cresol with methanol [23] and Friedel-Crafts alkylations [24].

In the present paper, the catalytic activity of MgFe mixed oxides derived from hydrotalcite precursors in the etherification of glycerol to diglycerol is reported. It has been studied the influence of the Mg/Fe molar ratio, the catalytic kinetic, the pretreatment of the catalysts and reusability of those catalysts, proving that these catalysts are highly active and selective in such reaction.

2. Experimental

2.1. Catalyst synthesis

The method of coprecipitation at constant pH [25] has been chosen to synthesize a series of Mg/Fe hydrotalcites. The Mg/Fe molar ratio was varied between 1 and 4, and the concentration of Mg + Fe was fixed at 1 M. The pH was maintained at a value of 10 by using a precipitant solution of NaOH/Na₂CO₃ with a concentration of OH⁻ and CO₃²⁻ of 2 and 0.125 M, respectively. Both solutions were dropped wisely in a flask containing 100 mL of distilled water, under vigorous stirring. The synthesis was carried out at room temperature and the precursor solution was aged during 24 h. The resulting solids were filtered, deeply rinsed with distilled water and dried at 65 °C. The solids were labelled as MgFex, where x stands for the Mg/Fe molar ratio. Prior the catalytic test, the hydrotalcites were activated in a tubular furnace at 450 °C during 15 h, under a helium flow, to transform them in the corresponding MgFe mixed oxides (MgFeOx). Pure Mg(OH)₂ was synthesized by using this same methodology. Na₂CO₃ (Merck) was also used, as received, for comparison, since it is the industrial catalyst. MgO catalyst was prepared from thermal treatment of Mg(OH)₂ at 450 °C under a helium flow.

2.2. Catalyst characterization

Elemental analysis was performed on a PERKIN-ELMER 2400 CHN with a LECO VTF900 pyrolysis oven. Mg, Fe and Na contents have been determined by ICP-AES by using a Perkin Elmer (model ELAN DRC-e) spectrometer. Powder XRD patterns were obtained by using a Siemens D5000 automated diffractometer, over a 2θ range with Bragg-Brentano geometry using the Cu Kα radiation and a graphite monochromator. X-ray photoelectron spectroscopy (XPS) studies were performed with a Physical Electronics PHI 5700 spectrometer equipped with a hemispherical electron analyzer (model 80-365B) and a Mg Kα (1253.6 eV) X-ray source. High-resolution spectra were recorded at 45° take-off-angle by a concentric hemispherical analyzer operating in the constant pass energy mode at 29.35 eV, using a 720 mm diameter analysis area. Charge referencing was done against adventitious carbon (C 1s at 284.8 eV). The pressure in the analysis chamber was kept lower than 5 × 10⁻⁶ Pa. PHI ACCESS ESCA-V6.0 F software package was used for data acquisition and analysis. A Shirley-type background was subtracted from the signals. Recorded spectra were always fitted using Gauss-Lorentz curves in order to determine more accurately the binding energy of the different element core levels.

N₂ adsorption-desorption isotherms at -196 °C were obtained using an ASAP 2020 model of gas adsorption analyzer from Micromeritics, Inc. Prior to N₂ adsorption, the sample were evacuated at 450 °C (heating rate 10 K min⁻¹) for 18 h. Pore size distribution and pore volume were calculated with the BJH method.

Thermogravimetric and differential thermal analyses (TG-DTA) were performed on a Pyris-Diamond PerkinElmer apparatus. The temperature was varied from room temperature up to 1000 °C, at a heating rate of 10 K min⁻¹ with a flux of nitrogen of 100 mL min⁻¹ using a mass around 15 mg.

The basicity was studied by temperature-programmed desorption of CO₂. Samples (100 mg) were pretreated under a helium stream at 450 °C for 1 h (2 K min⁻¹, 100 mL min⁻¹). Then, temperature was decreased until 100 °C, and a flow of pure CO₂ (50 mL min⁻¹) was subsequently introduced into the reactor during 1 h. The CO₂-TPD was carried out between 100 and 800 °C under a helium flow (10 K min⁻¹, 30 mL min⁻¹), and evolved CO₂ was analyzed by an on-line gas chromatograph (Shimadzu GC-14A) provided with a TCD, after passing by an ice-NaCl trap to eliminate any trace of water. Temperature-programmed desorption of ammonia (NH₃-TPD) was carried out to evaluate the total acidity of the catalysts. After cleaning the materials with helium and adsorption of ammonia at 100 °C, the NH₃-TPD was performed between 100 and 550 °C with a heating rate of 10 K min⁻¹ by using a helium flow and maintained at 550 °C for 15 min. The evolved ammonia was analyzed by on-line gas chromatography (Shimadzu GC-14A) provided with a TCD detector.

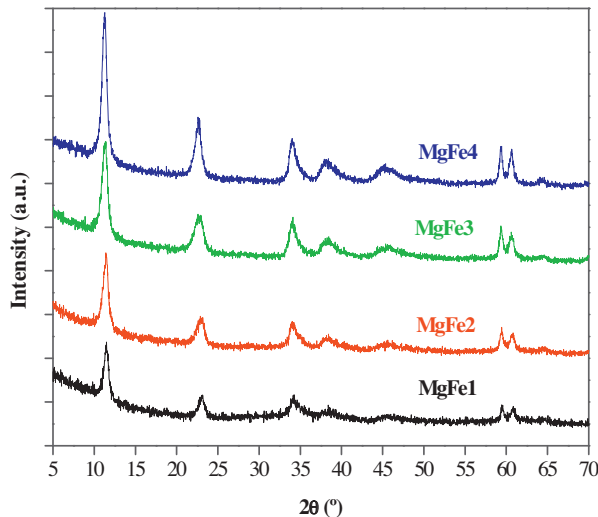
2.3. Catalytic reaction

The catalytic activity was evaluated in the etherification of glycerol (Aldrich) at 220 °C in a three-necked glass batch reactor without solvent, equipped with a water-cooled condenser coupled with a Dean-Stark system to remove the formed water, thermometer and vigorous stirring. The atmosphere of the reactor was kept inert by means of a N₂ flow of 15 mL min⁻¹. Before the reaction, catalysts were activated at different temperatures for 15 h (heating rate, 2 K min⁻¹), under a helium flow. The reaction was stopped at 24 h and catalysts were separated by filtration on a porous plate. Then, catalysts were washed deeply with hot water and ethanol. The reaction products were analyzed by means of gas chromatography. An aliquot (ca 80 mg) of the reaction mixture was dissolved in dried pyridine (Aldrich) and then N,O-bis(trimethylsilyl)trifluoroacetamide was added. This solution

Table 1

Chemical analysis and crystallographic parameters of as-synthesized MgFe hydroxylites.

Sample	Mg ^a (wt%)	Fe ^a (wt%)	Mg/Fe ^a (molar ratio)	C ^b (wt%)	N ^b (wt%)	c (Å)	a (Å)	d_{003} (Å)	Crystallite size (c) (nm)	Crystallite size (a) (nm)
MgFe1	10.4	22.6	1.1	1.7	0.0	23.2	3.1	7.7	12.5	29.5
MgFe2	14.7	20.1	1.7	2.0	0.2	23.3	3.1	7.8	11.9	25.4
MgFe3	19.5	15.7	2.9	1.8	0.7	23.4	3.1	7.8	10.6	19.9
MgFe4	20.9	13.7	3.6	1.7	0.9	24.1	3.1	7.9	12.8	24.7

^a Calculated from AA analysis.^b Calculated from CNH analysis.**Fig. 1.** XRD patterns of as-synthesized MgFe_x hydroxylites.

was aged in a stove at 60 °C during 1 h and analyzed in a gas chromatograph (Shimadzu GC model 14A) equipped with FID and a capillary silica fused TBR-14 column (Tecknchroma). The only detected products were unreacted glycerol, di- and tri-glycerol. The selectivities to the different products were calculated as the weight ratio of the respective product to the sum of products formed. The glycerol conversion was calculated as the ratio of the detected glycerol to the sum of the glycerol and products formed.

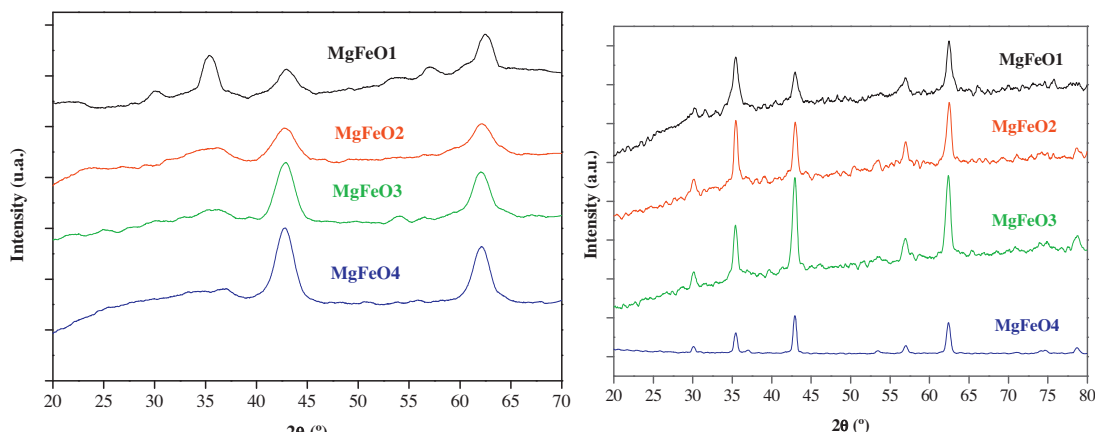
3. Results and discussion

3.1. Characterization of hydroxylite precursors and catalysts

The XRD patterns of MgFe_x hydroxylites exhibit the diffraction pattern characteristic of the hydroxylite structure, irrespective of

Mg/Fe molar ratio, with sharp and intense diffraction peaks due to basal planes, and broad and asymmetric peaks ascribed to non-basal planes (Fig. 1). Thus, the sharp peaks at $2\theta \approx 11^\circ$, 23° and 34° correspond to the (0 0 3), (0 0 6) and (0 0 9) planes, respectively, indicating a well-formed crystalline layered structure with rhombohedral symmetry. No other crystalline phases, such as Fe(OH)₃ or Mg(OH)₂, were detected in the XRD patterns. On the other hand, the crystallinity increases with the Mg content, as can be inferred from the intensification of the diffraction peak corresponding to the (0 0 1) planes. The basal spacing (d_{003} reflection) values have confirmed the presence of carbonate anions in the interlayer region [26,27]. The MgFe4 hydroxylite shows a higher basal spacing among the synthesized samples, and higher than those reported for carbonate anions as compensating anions in the interlayer region [28]. This fact could be ascribed to the concomitant presence of nitrate anions, as could point out the highest nitrogen content found by CHN analysis (Table 1), because it has been previously reported that the basal spacing is higher in the presence of nitrate anions [17].

The corresponding lattice parameters and d_{003} basal spacing are presented in Table 1, together with the average crystallite sizes, obtained from the full width a half maximum (FWHM) of diffraction peaks corresponding to (0 0 3) and (1 1 0) planes, by using the Scherrer equation. The unit cell parameter, a , is the average distance between two metal ions within the layers, and it has been calculated from the d -spacing of the (1 1 0) reflection ($a = 2d_{110}$). The c parameter is three times the distance between adjacent hydroxide and it has been also calculated from the (0 0 3) reflection ($c = 3d_{003}$). The a parameter barely changes with the decrease of the Mg/Fe molar ratio, since the ionic radius of Fe³⁺ and Mg²⁺ cations are very similar: 0.69 and 0.65 Å, respectively [23,29]. In return, the c parameter shows a significant reduction as the Mg/Fe molar ratio decreases, which is consistent with the increase in Coulombic attractive forces between the negatively charged interlayer anions and the positively charged brucite-like layers with the increasing of Fe³⁺ cations. Therefore, the layers are packed closer with lower Mg/Fe molar ratio [30,31]. The crystallite sizes are longer in

**Fig. 2.** (a) XRD patterns of MgFeO_x mixed oxides derived from MgFe_x hydroxylites calcined at 450 °C and (b) XRD patterns of MgFeO_x mixed oxides derived from MgFe_x hydroxylites calcined at 800 °C.

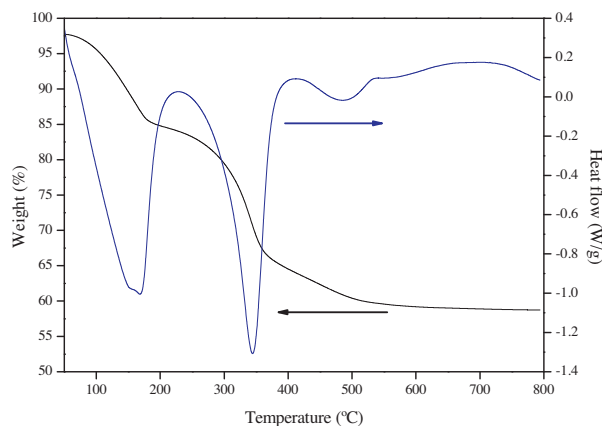


Fig. 3. DTA-TG curves of the as-synthesized MgFe_3 hydroxylate.

a direction, which it is expected from the well-known platelet-like morphology of hydroxylate crystallites [32].

The as-synthesized samples were calcined under a helium flow at 450°C in order to transform them into the respective MgFeO_x mixed oxides (Fig. 2a). This thermal treatment leads to the structural collapse with remarkable structural changes. All of them exhibit XRD patterns quite similar to that of MgO phase (periclase), but with broad peaks ($2\theta \approx 43^\circ, 63^\circ$) indicating poor crystallinity. On the other hand, the sample with Mg/Fe molar ratio of 1 shows other broad peaks at ca. $2\theta \approx 30^\circ, 35^\circ$ and 57° , which can be ascribed to the spinel MgFe_2O_4 phase [23,24], although the presence of Fe_3O_4 cannot be ruled out since these two phases show a similar XRD patterns [23], and thermal treatment in inert atmosphere could result in a partial reduction of Fe^{3+} . When the temperature of thermal treatment is raised to 800°C , all the samples exhibit the diffraction peaks of the spinel phase, irrespectively of the Fe content (Fig. 2b).

Thermogravimetric (TG) and Differential Thermal Analysis (DTA) curves are very similar, and Fig. 3 displays, as an example, those corresponding to the MgFe_3 hydroxylate. These results are in good agreement with those from the literature [18–21,24,25]. The differences are only observed in the intensity of the three steps of weight loss and the corresponding endothermic effects. The first stage accounts for the removal of the water loosely bounded in the interlayer region, with no significant differences among the studied hydroxylates, either the peak temperatures or weight loss. The second weight loss is associated to dehydroxylation of the brucite layers and decomposition of the interlayer anions with the concomitant structural collapse, as evidenced the XRD patterns, leading to the formation of metal oxides. The third one corresponds to ca. 5 wt% of weight loss. By means of evolved gaseous analysis by mass spectroscopy (Appendices A and B, Fig. S1), neither mass 44 nor 18 were detected, therefore the thermal processes involved in the decarbonation and dehydroxylation have finished before 500°C . In return, a peak corresponding to the mass 32 was detected pointing out a release of oxygen and partial reduction of the $\text{Fe}(\text{III})$ in the mixed oxides could take place [33].

The textural properties have been determined from nitrogen adsorption–desorption isotherms at -196°C of the MgFeO_x , after calcination at 400°C , and the main textural parameters are shown in Table 2. The shapes of all isotherms are type IV according to the IUPAC classification (Supplementary Information, Fig. S2), typical of mesoporous materials [34]. The analysis of the hysteresis loops has been used to describe the pore structure of porous solids [17,19,25,35–38]. The hysteresis loops of calcined hydroxylates resemble to type H3 hysteresis, which is usually found in materials

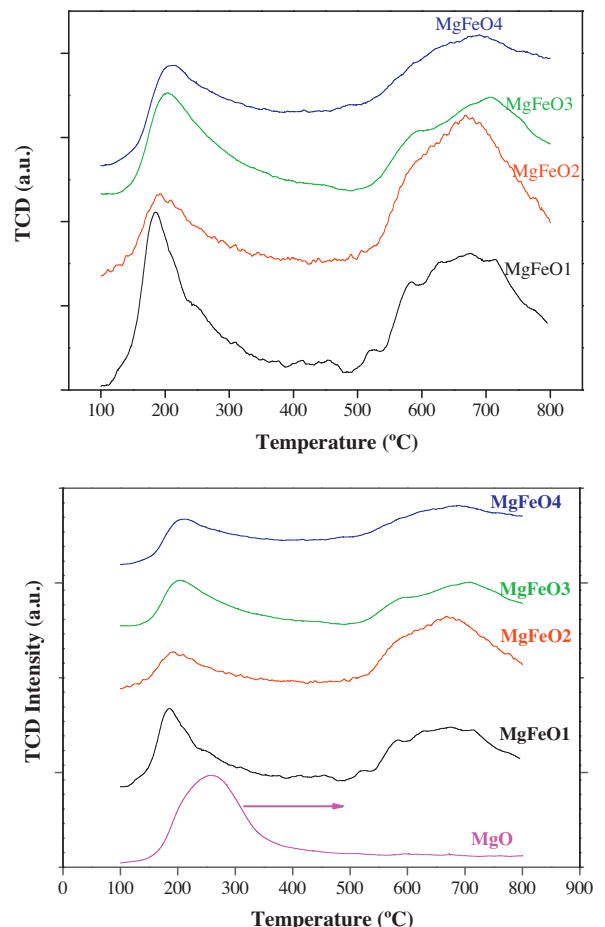


Fig. 4. (a) TPD-NH₃ curves of the MgFeO_x catalysts and (b) TPD-CO₂ curves of the MgFeO_x catalysts.

consisting of aggregates of particles forming slit-shaped pores with non uniform size or shape [39].

The pore size distributions of the MgFeO_x samples are relatively broad, extending from 2 to 70 nm with a maximum at around 15 nm (Supplementary Information, Fig. S2). They present a bimodal pore size distribution. Thus, the calcined hydroxylates show pores in the range of 2–3.5 nm, which formation is favoured by the evolved gaseous products generated during the thermal decomposition of the interlayer anions. Such mechanism of decomposition is known as “cratering” [40] and it is responsible of the intraporosity of particles. On the other hand, a second pore size bands ranges from 4 to 70 nm, and these pores are formed as result of the collapse of the plate like particles, provoking the interparticle porosity characteristic of most clay materials [41]. The textural parameters of the MgFeO_x samples were observed to decrease with an increase in Fe loading. The highest pore volume found in the MgFeO_3 and MgFeO_4 samples could be ascribed to their highest porosity in the range of 4–70 nm.

The acid-base properties of catalysts play an important role in their catalytic performance in the etherification of glycerol. In fact, the acid sites may conduct the selectivity of the reaction towards acrolein and the basic ones are involved in the etherification of glycerol, and therefore the production of polyglycerols. The acid sites have been evaluated by NH₃-TPD analysis (Table 2 and Fig. 4a). The incorporation of Fe^{3+} cations in the brucite structure modified drastically the acid properties of the resulting mixed oxide. Actually, the MgO sample does not show detectable acid sites, whereas the incorporation of Fe^{3+} cations produces a broad heterogeneous distribution of acid sites. The concentration of acid sites increases

Table 2Textural parameters of MgFeO_x metal oxides.

Sample	S _{BET} (m ² /g)	V _p (cm ³ /g)	dp (av) (nm)	Acidity		^b Basicity	
				(μmol NH ₃ /g)	(μmol NH ₃ /m ²)	(μmol CO ₂ /g)	(μmol CO ₂ /m ²)
MgFeO1	112	0.214	7.1	623	5.6	265	2.4 (0.42)
MgFeO2	206	0.483	8.8	728	3.5	217	1.1 (0.31)
MgFeO3	256	0.607	8.5	653	2.6	167	0.7 (0.27)
MgFeO4	221	0.665	10.8	381	1.7	184	0.8 (0.47)
^a MgO	324	0.827	5.6	—	—	930	2.9 (—)

^a The acidity of MgO sample was not detected by means of TPD-NH₃.^b In brackets the ratio of specific basicity/acidity determined by means of CO₂-TPD and NH₃-TPD.

with decreasing of Mg/Fe molar ratio, reaching a maximum value for the catalyst MgFeO2. The lower acidity of the MgFeO1 could be ascribed to its lower S_{BET}, as previously reported by Tu et al. [42] in the study of the acidity of MgFe mixed oxides by microcalorimetry of NH₃ adsorption. These authors found the highest adsorption heat and ammonia coverage for a sample with Mg/Fe molar ratio of 1 and the lowest to the MgO sample. Pavel et al. [43] reported that MgFeAlO mixed oxide showed that the total number of acid sites was increased due to the presence of a segregated spinel or Fe₂O₃ phase. However, León et al. [20] have reported a MgFe mixed oxide with Mg/Fe molar ratio close to 3 with negligible ammonia adsorption. The authors ascribed this low acidity value to the impossibility of Fe³⁺ ions to occupy a tetrahedral site because of its larger ionic diameter.

The CO₂-TPD profiles of calcined hydrotalcites (Fig. 4b) clearly reveal that the incorporation of Fe³⁺ provokes a drastic change in the CO₂-TPD profile, as well as in the concentration of basic sites (Table 2). MgO only shows an intense peak centred around 275 °C, whereas the calcined hydrotalcites exhibit two well resolved peaks, one at low temperature with the maximum at 200 °C and another one at 700 °C. Based on these results, the high temperature peak could be ascribed to strong basic sites generated by the presence of iron ions in the MgO structure, whereas the low temperature peak could be attributed to the periclase structure itself. In mixed oxides, the partial substitution of Mg²⁺ by Fe³⁺ generates an excess of positive charge which is compensated by cationic vacancies [44]. The neighboured oxygen anions to these structural defects are unsaturated and provide the strongest basic sites. On the basis of CO₂ adsorption coupled to FTIR analysis, it has been reported in the literature [45–48] that CO₂ adsorption on surface hydroxyl groups (low strength basic sites) generates bicarbonate ions, whereas carbonate species are formed on O²⁻ ions (strong basic sites) [20]. Therefore, the peak at low temperature could be ascribed to bicarbonates species desorption whereas the peak at high temperature could be derived from carbonates species desorption. Moreover, the asymmetry of the peak centred at 700 °C would point out the formation of different types of carbonates, i.e. unidentate (strong basic site), bidentate, chelating and bridging carbonates (medium strength basic site) [20].

Regarding the concentration of basic sites, they decrease for higher Mg/Fe molar ratio, but in all cases they are lower than MgO. This fact is related to the increase of unsaturated oxygen anions [23], which are Lewis base sites, as the Fe loading is increased [42].

In summary, these mixed oxides show features related to both acid and base sites, which surface concentration increases with the iron loading. Besides, the density of surface acid and basic sites, namely the concentration per square meter, follows the same trend, i.e. the MgFeO1 shows the highest density, although the surface basic/acid sites ratio does not vary irrespectively of the Mg/Fe molar ratio.

The surface characteristics of the as-synthesized hydrotalcites and the mixed oxides have been studied by means of XPS. It has been evaluated the signals in the C 1s, O 1s, Mg 2p and Fe 2p

regions and it has been calculated the surface concentration of these elements. The XPS results collected in Table 3.

Regarding the C 1s signal (Supplementary Information, Fig. S3), the MgFe hydrotalcites exhibit two bands: adventitious carbon at 284.7–284.9 eV and carbonates at 287.8–289.0 eV. The mixed oxides MgFeO_x still show the presence of the carbonates even after the thermal treatment at 450 °C, which could be due to the existence of remaining strong bonded carbonates, although the contamination by adsorbed CO₂ during the sample handling cannot be ruled out.

In the O 1s region (Supplementary Information, Fig. S3), the as-synthesized hydrotalcites display an asymmetric band that can be deconvoluted into two bands at 529.5 and 531.2 eV, which could be ascribed to the presence of O²⁻ and species like OH or carbonates groups, respectively. The thermal treatment of the hydrotalcites to generate the MgFe mixed oxides provokes an increase in the intensity of the band at 529.5 eV and a decrease in the intensity of the

Table 3Binding Energies of C 1s, O 1s, Mg 2p y Fe 2p of the as-synthesized hydrotalcites, MgFeO_x catalysts before and after catalytic test.

*Sample	C 1s (eV)	O 1s (eV)	Mg 2p (eV)	Fe 2p (eV)
MgFe1	285.4 (83.3)	529.6 (14.3)	49.4	710.3
	288.5 (16.7)	531.1 (85.7)		
MgFe2	284.8 (67.6)	529.7 (17.2)	48.9	711.2
	289.0 (32.4)	531.4 (82.8)		
MgFe3	284.9 (57.2)	529.5 (6.7)	49.5	711.6
	288.8 (42.8)	531.2 (93.3)		
MgFe4	284.9 (70.0)	529.5 (5.7)	49.5	711.1
	288.8 (30.0)	531.2 (94.3)		
**Sample	C 1s (eV)	O 1s (eV)	Mg 2p (eV)	Fe 2p (eV)
MgFeO1	284.9 (69.9)	529.6 (57.0)	48.9	710.6
	289.7 (30.1)	531.3 (36.7)		
MgFeO2	284.9 (69.1)	529.4 (45.5)	48.9	710.5
	288.9 (30.9)	531.1 (45.4)		
MgFeO3	285.0 (69.0)	529.4 (48.2)	48.9	710.6
	288.9 (31.0)	531.2 (42.0)		
MgFeO4	284.9 (63.9)	529.4 (48.5)	48.8	710.4
	289.0 (36.1)	531.2 (42.1)		
***Sample	C 1s (eV)	O 1s (eV)	Mg 2p (eV)	Fe 2p (eV)
MgFeO1	284.8	530.2 (87.9)	48.8	709.7
		532.1 (12.1)		
MgFeO2	284.8 (93.8)	530.3 (85.6)	49.0	709.4
	287.2 (6.2)	532.1 (14.4)		
MgFeO3	284.8 (86.5)	530.5 (89.4)	48.9	709.3
	287.9 (13.5)	531.8 (10.6)		
MgFeO4	284.0 (39.1)	530.2 (66.7)	48.8	708.2
	285.2 (60.9)	531.8 (33.1)		

^{*} As-synthesized hydrotalcites.^{**} Calcined hydrotalcites at 450 °C.^{***} XPS results after catalytic test.

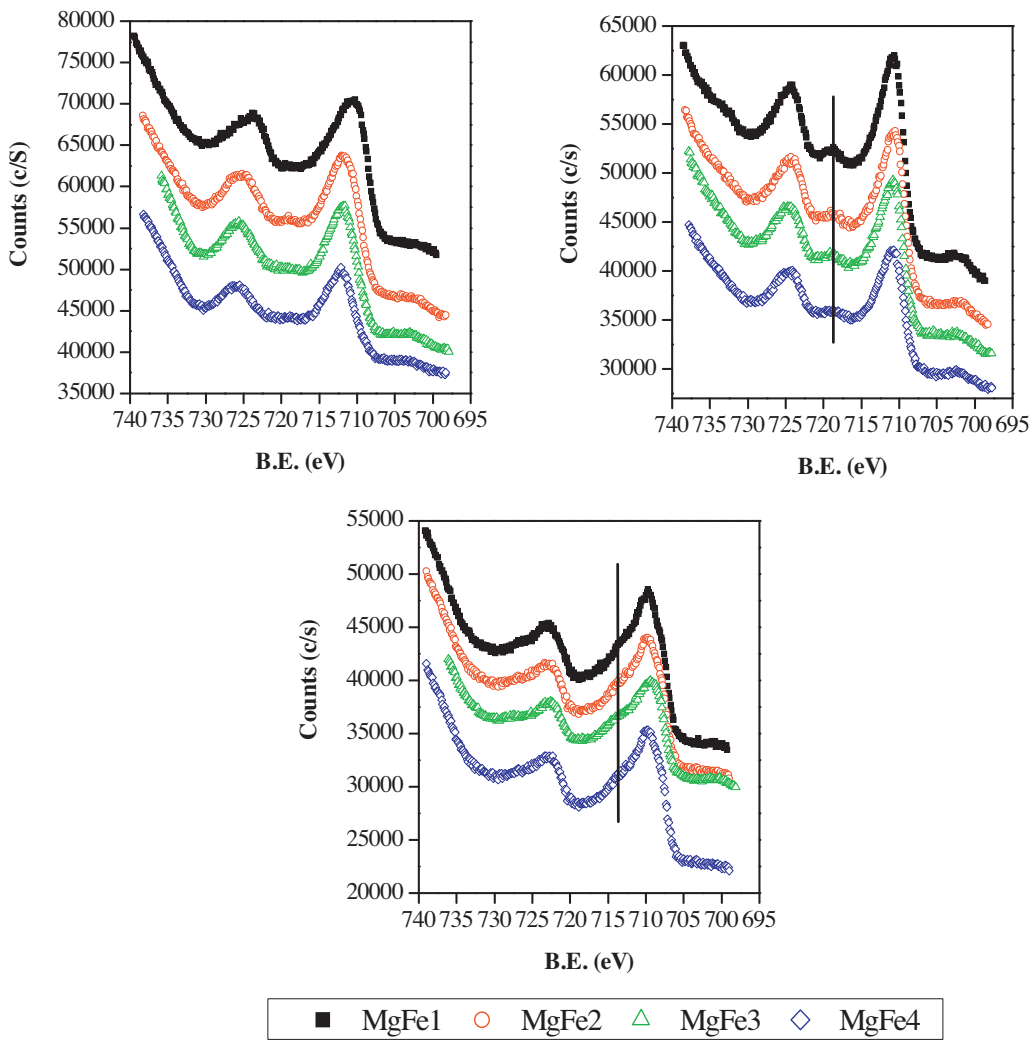


Fig. 5. Fe2p core level of the as-synthesized hidrotalcites, MgFeOx catalysts before and after reaction (from left to right and top to bottom).

band at 531.2 eV. This fact remarks the dehydroxilation and decarbonation of the as-synthesized hidrotalcites, as ATD-TG analysis showed, and it points out the increase of the strong basic centres on the surface of mixed oxides expressed in the presence of O²⁻ species. Moreover, the increase in the Fe loading is associated to an increase in the band ascribed to the O²⁻ ions. The XPS results corroborate that the sample with the lower Mg/Fe molar ratio showed the highest CO₂ adsorption at the highest temperatures measured by CO₂-TPD.

Finally, in the Fe 2p region, the as-synthesized hidrotalcites and the mixed oxides show a broad Fe 2p_{3/2} peak, which broadening is attributed to multiplet splitting and shake-up phenomena [49]. The presence or absence of shake up satellite near of the photoelectron peak provides information about the oxidation state of iron [50]. If the iron is at the oxidation state (+II) the satellite is a shoulder in the photoelectron peak, whereas in the case of oxidation state (+III) the satellite peak is a discernible peak at about 8 eV from the photoelectron peak and, finally if oxidation state of the iron is (0) the satellite peak is absent. The photoelectron Fe 2p_{3/2} peak of the as-synthesized hidrotalcites is ranged between 709.9 and 712.0 eV. These binding energies together the shape of spectra are indicative of the presence of Fe(III), as reported for compounds like FeOOH and Fe(OH)₃ [50]. When the hidrotalcites are converted in mixed oxides by the thermal treatment at 450 °C, the Fe 2p spectra display the photoelectronic features of iron at oxidation state (+III), that is, the

binding energy of the Fe 2p_{3/2} peak and the presence of a detectable satellite peak at 8 eV from the Fe 2p_{3/2} peak (Fig. 5) [51–54].

3.2. Catalytic results

Currently, much attention is being paid to the etherification of glycerol to polyglycerol, under heterogeneous conditions, since this process takes advantages, such as easiness of catalyst separation from the reaction medium and catalyst reutilization. However, compared to homogeneous catalysts, the main drawbacks of solid catalysts are related to lower catalytic activity, the requirement of more drastic reaction conditions and the possible leaching in the reaction media. In this etherification process, one of the main catalytic goals is to address the selectivity towards di-glycerol and tri-glycerol, since these oligomers are starting materials for the food and cosmetic industries. In this present work, the etherification of glycerol to polyglycerols using heterogeneous catalysis was carried out in a batch reactor, without solvent, at 220 °C under a continuous nitrogen flow, during 24 h under atmospheric pressure. Under these experimental conditions, di-glycerols and tri-glycerols were only detected.

Fig. 6a shows the catalytic results obtained over MgFeOx catalysts, 2 wt% at 220 °C, together with those of commercial Na₂CO₃, MgO and Fe(OH)₃ for comparison. Na₂CO₃ was the most active catalyst under these experimental conditions, reaching 100% glycerol

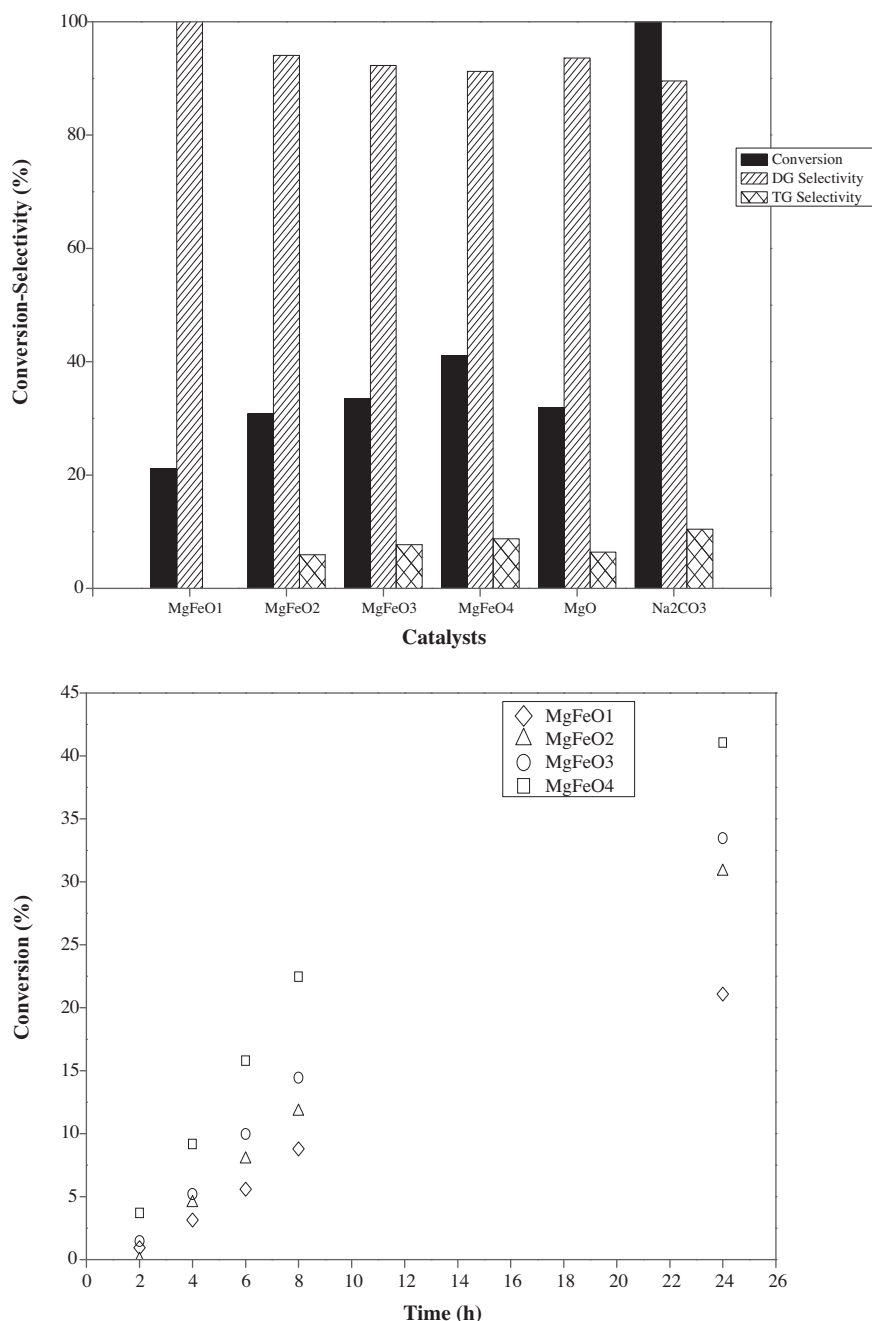


Fig. 6. Catalytic performance MgFeO_x catalysts: (a) glycerol conversion and diglycerol and triglycerol selectivity; (b) glycerol conversion versus reaction time (reaction conditions: glycerol = 15 g, catalyst weight = 300 mg; temperature = 220 °C, reaction time: 24 h).

conversion after 24 h of reaction as previous results have shown [9]. It is noteworthy that its catalytic activity was higher than that obtained with a MgO prepared by activation of the corresponding nitrate at 700 °C [11]. The MgFeO_x mixed oxides show a gradual increase of the catalytic activity with the Mg/Fe molar ratio, being the MgFeO₄ catalyst the most active. Thus, glycerol conversion varies between 21.1% and 41.1%, after 24 h time on stream. None of the MgFeO_x catalysts reached full conversion of glycerol under these experimental conditions. The catalytic behaviour seems to be related to both the acid-basic properties and structural stability of catalysts (as inferred from the superficial Mg/Fe atomic ratio). The MgFeO₄ catalyst shows the higher specific basicity/acidity ratio (see Table 2), whereas the surface Mg/Fe atomic ratio (Table 4) after the catalytic reaction is hardly affected. The rest of catalysts

Table 4
Mg/Fe atomic ratio determined by means of XPS analysis and Mg/Fe molar ratio determined by ICP-AES analysis.

Sample	^a Mg/Fe			
	MgFe _x	MgFeO _x	[*] MgFeO _x	^b Mg/Fe (%)
MgFe1	0.886	0.899	0.474	1.0
MgFe2	1.602	1.348	0.692	1.7
MgFe3	3.218	2.372	1.965	2.9
MgFe4	3.632	3.125	3.190	3.6

^a Measure from XPS analysis.

^b Measure from ICP-AES.

* Data after catalytic tests.

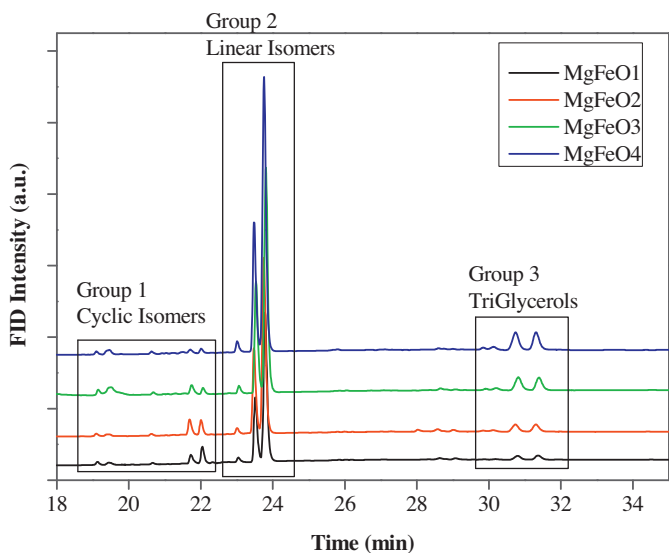


Fig. 7. Chromatograms of the reaction mixture after 24 h as function of the MgFeO_x catalysts.

evidence a significant reduction of the exposed iron, being nearly 50% for the MgFeO₂ and MgFeO₁ catalysts (Table 4). It is noteworthy to point out that all catalysts present a similar carbon deposition degree on their surfaces, so this decrease in the surface Mg/Fe atomic ratio is not associated to carbon deposition. Thus, this fact could point out a partial segregation of iron species from the MgFeO framework during the catalytic process. The extraction of the Fe³⁺ from the periclase structure could be related to the partial reduction of Fe³⁺ to Fe²⁺, as it is observed by XPS analysis, since the Fe 2p core level of the mixed oxides (Fig. 5) reveals a shift to lower binding energies, roughly 1 eV. Furthermore, the satellite peak appears as a shoulder of the Fe 2p_{3/2} photoelectronic peak, thus corroborating the partial reduction of Fe³⁺ to Fe²⁺. Therefore, the existence of extra-framework iron could be related to the lower catalytic performance of catalysts with Mg/Fe molar ratio lower than 4.

Regarding the selectivity (Fig. 6a), all these catalysts display selectivity towards diglycerol greater than 90%, which declines as glycerol conversion is increased. This selectivity results are similar to those reported by Richter et al. [55] and Clacens et al. [9] for similar levels of glycerol conversion. It is well known that oligomerisation of glycerol can lead to dimers, trimers and higher oligomers (Supplementary Information, Scheme S1). Moreover, once a dimer is formed, cyclic products can be produced as result of intramolecular ring closure reactions [56] and therefore the composition of a polyglycerol mixture is extremely complex. Taking into account the chromatograms of standard reference compounds, the chromatogram peaks of reaction mixture after the silylation process have been grouped in three classes, which have been labelled as Group 1, 2 and 3 (Fig. 7). The Group 1 included those species eluted between 20 and 22 min, the Group 2 included those peaks between 22 and 23 min and Group 3, those between 30 and 31 min. The Group 1 (Supplementary Information Scheme S1) consisted of small peaks associated to the existence of cyclic diglycerol isomers. These cyclic isomers only have two hydroxyl groups to react and therefore they are trimethyl-disilyl derivatives and as consequence their molecular weight are lower and they eluted at lower retention times. The peaks included in the Group 2 are the most intense, and hence these isomers are more abundant. These are linear isomers (Supplementary Information Scheme S1), such as α,α -diglycerol, α,β -diglycerol and β,β -diglycerol [56]. The linear diglycerol isomers have four hydroxyl groups and therefore their molecular weight is higher than such cyclic isomers and then they

eluted after the cyclic ones. Based on reaction probabilities [57], the α,α -diglycerol will be formed more readily than the branched isomers, and therefore the highest peak can be ascribed to that isomer. Finally, the Group 3 accounts for the triglycerol isomers whose intensity is lower than that of linear isomers

The etherification of glycerol is a shape-selective reaction in which the pore framework plays an important role to lead the selectivity to a particular product, in this case to diglycerol. The textural analysis of the catalysts has proven that these catalysts possess pore diameters large enough to facilitate the diffusion of glycerol and the reaction products. Indeed, the sizes of glycerol isomers [57] range between 0.667 and 0.753 nm for α,α -diglycerol and β,β -diglycerol, respectively. Therefore, the reaction may occur into the pores of the mixed oxides and the existence of large pore diameters in all cases is responsible of the similar selectivity values observed in all cases. Although, from a qualitative point of view and bearing in mind that the statistical distribution of the $\alpha,\alpha:\alpha,\beta:\beta,\beta$ dyglycerol isomers ratios might be 57:29:14 [57], the actual ratio is quite shifted to the formation of the (α,α) isomer. This means that these catalysts favour the synthesis of those diglycerol isomers.

It has been previously reported that the more active catalysts shows basic features and acidic ones address the selectivity towards the acrolein formation [5,11]. Weckhuysen et al. [11] also showed that the Lewis acid sites of the alkaline-earth metals played a role in the activation of glycerol molecules. In this mechanism, a basic centre attacks a hydroxyl group of a glycerol molecule, extracting a proton, whereas an unsaturated metal site on the catalyst surface is able to activate a hydroxyl group of other glycerol molecule, which is then attacked by the nucleophilic oxygen of the former glycerol molecule yielding the diglycerol molecule. This acid–base bifunctional mechanism has been postulated for other catalytic reactions, in which mixed oxides derived from hydrotalcites have been used [23,25,43,58]. This mechanism could be involved in presence of MgFeO_x catalysts where acid and basic sites are present, as demonstrated by NH₃-TPD and CO₂-TPD.

The influence of reaction time in the catalytic performance (Fig. 6b) shows that the catalytic performance of MgFeO₄ catalyst is the highest in the whole range of time. It is noteworthy that the catalysts require an activation period before showing any catalytic activity. The selectivity to diglycerol is 100%, at least within the first eight hours, and then triglycerol becomes measurable.

The main advantage of using heterogeneous versus homogeneous catalysts is the possibility of reusing. For that, the active phase must not be leached to the reaction medium. Thus, the organic phase was analyzed by ICP-AES to detect any trace of iron or magnesium. The absence of metals in the reaction medium, even with those catalysts showing a decrease of Mg/Fe atomic ratio, confirms the stability of the solid catalysts. Therefore, the Mg/Fe atomic ratio depletion observed after the catalytic test is not accounted for the leaching of Mg or Fe but it is explained by the segregation of iron species.

4. Conclusions

Magnesium iron hydrotalcites with variable Mg/Fe molar ratio, ranging from 1 to 4, have been prepared as precursors of MgFe mixed oxides, which have demonstrated to be active in the selective etherification of glycerol to yield mainly diglycerol. The catalytic behaviour seems to be influenced by the stability of iron in the structure of MgO oxide. This is achieved with the Mg/Fe molar ratio of 4. The rest of catalysts show a noticeable decrease of Mg/Fe atomic ratio, as determined by XPS, after the catalytic test, indicating a partial segregation of iron species over the MgO surface. These catalysts display a catalytic selectivity to diglycerol (<90%) without significant differences between the tested catalysts. Moreover, the catalysts do not show any leaching of the Fe or Mg in the

reaction mixture after the catalytic test, which is important when considering their reuse in several catalytic cycles.

Acknowledgements

The authors are grateful to financial support from the Spanish Ministry of Science and Innovation (ENE2009-12743-C04-03 project), Junta de Andalucía (P09-FQM-5070) and FEDER funds. RMT would like to thank this Ministry of Science and Innovation for the financial support under the Program Ramón y Cajal (RYC-2008-03387).

Appendix A. Supplementary data

Supplementary material related to this article can be found, in the online version, at <http://dx.doi.org/10.1016/j.apcata.2013.10.051>.

References

- [1] <<http://www.ebb-eu.org/stats.php>>.
- [2] M. Pagliaro, R. Ciriminna, H. Kimura, M. Rossi, C. Della Pina, *Angew. Chem. Int. Ed.* **46** (2007) 4434–4440.
- [3] B. Katryniok, S. Paul, V. Bellière-Baca, P. Rey, F. Dumeignil, *Green Chem.* **12** (2010) 2079–2080.
- [4] C.H. Zhou, J.N. Beltramini, Y.-X. Fan, G.Q. Lu, *Chem. Soc. Rev.* **37** (2008) 527–549.
- [5] M.V. Sivaiah, S. Robles-Manuel, S. Valange, J. Barrault, *Catal. Today* **198** (2012) 305–313.
- [6] A. Martin, M. Richter, *Eur. J. Lipid Sci. Technol.* **113** (2011) 100–117.
- [7] M. Ayoub, M.S. Khayoon, A.Z. Abdullah, *Bioresour. Technol.* **112** (2012) 308–312.
- [8] J.-M. Clacens, Y. Pouilloux, J. Barrault, *Stud. Surf. Sci. Catal.* **143** (2002) 687–695.
- [9] J.-M. Clacens, Y. Pouilloux, J. Barrault, *Appl. Catal., A* **227** (2002) 181–190.
- [10] J. Barrault, J.-M. Clacens, Y. Pouilloux, *Top. Catal.* **27** (2004) 137–142.
- [11] A.M. Ruppert, B.M. Weckhuysen, J.D. Meeldijk, B.W.M. Kuipers, B.H. Erné, *Chem. Eur. J.* **14** (2008) 2016–2020.
- [12] Z. Gholami, A.Z. Abdullah, K.-T. Lee, J. Taiwan Inst. Chem. Eng. **44** (2013) 117–122.
- [13] C. García-Sancho, R. Moreno-Tost, J.M. Mérida-Robles, J. Santamaría-González, P. Maireles-Torres, *Catal. Today* **167** (2011) 84–90.
- [14] M.R. Anuar, A.Z. Abdullah, M.R. Othman, *Catal. Commun.* **32** (2011) 67–70.
- [15] D. Tichit, F. Fajula, *Stud. Surf. Sci. Catal.* **125** (1999) 329.
- [16] F. Cavani, F. Triffirò, A. Vaccari, *Catal. Today* **11** (1991) 173–301.
- [17] K.S. Triantafyllidis, E.N. Peleka, V.G. Komvokis, P.P. Mavros, *J. Colloid Interface Sci.* **342** (2010) 427–436.
- [18] Y. Yang, N. Gao, Y. Deng, S. Zhou, *Appl. Clay Sci.* **65–66** (2012) 80–86.
- [19] J.S. Valente, J. Hernández-Cortez, M.S. Cantu, G. Ferrat, E. López-Salinas, *Catal. Today* **150** (2010) 340–345.
- [20] M. León, E. Díaz, A. Vega, S. Ordóñez, A. Auoux, *Appl. Catal., B* **102** (2011) 590–599.
- [21] P. Kustrowski, A. Rafalska-Lasocha, D. Majda, D. Tomaszewska, R. Dziembaj, *Solid State Ionics* **141–142** (2001) 237–242.
- [22] Y. Ohishi, T. Kawabata, T. Shishido, K. Takaki, Q. Zhang, Y. Wang, K. Nomura, K. Takehira, *Appl. Catal., A* **288** (2005) 220–231.
- [23] V. Crocellà, G. Cerrato, G. Magnacca, C. Morterra, F. Cavani, S. Cocchi, S. Passeri, D. Scagliarini, C. Flego, C. Perego, *J. Catal.* **270** (2010) 125–135.
- [24] N. Tahir, Z. Abdelsadek, D. Hallache, S. Saadi, R. Chebou, O. Cherifi, K. Bachari, *Surf. Interface Anal.* **40** (2008) 254–258.
- [25] M. León, E. Díaz, S. Bennici, A. Vega, S. Ordóñez, A. Auoux, *Ind. Eng. Chem. Res.* **49** (2010) 3663–3670.
- [26] S.K. Sharma, P.A. Parikh, R.V. Jasra, *Appl. Catal., A* **386** (2010) 34–42.
- [27] C.M. Jinesh, C.A. Antonyraj, S. Kannan, *Appl. Clay Sci.* **48** (2010) 243–249.
- [28] M.A. Ulibarri, M.J. Hernández, J. Cornejo, *Thermochim. Acta* **113** (1987) 79–86.
- [29] O.P. Ferreira, O.L. Alves, D.X. Gouveia, A.G. Souza Filho, J.A.C. de Paiva, J.M. Filho, *J. Solid State Chem.* **177** (2004) 3058–3060.
- [30] J.S. Valente, H. Pfeiffer, E. Lima, J. Prince, J. Flores, *J. Catal.* **279** (2011) 196–204.
- [31] M. Vučelic, W. Jones, G.D. Moggridge, *Clays Clay Miner.* **45** (1997) 803–813.
- [32] J. Pérez-Ramírez, S. Abelló, N.M. van der Pers, *Chem. Eur. J.* **13** (2007) 870–879.
- [33] R.L. Frost, K.L. Erickson, *J. Therm. Anal. Calorim.* **76** (2004) 217–225.
- [34] K.S.W. Sing, D.H. Everett, R.W. Haul, L. Moscou, R.A. Pierotti, J. Rouquérol, T. Siemieniewska, *Pure Appl. Chem.* **57** (1985) 603–619.
- [35] S.K. Sharma, P.K. Kushwaha, V.K. Srivastava, S.D. Bhatt, R.V. Jasra, *Ind. Eng. Chem. Res.* **46** (2007) 4856–4860.
- [36] E. Angelescu, O.D. Pavel, R. Birjega, M. Florea, R. Zavoianu, *Appl. Catal., A* **341** (2008) 50–57.
- [37] P. Kustrowski, L. Chmielarz, E. Bozek, M. Sawalha, F. Roessner, *Mater. Res. Bull.* **39** (2004) 263–281.
- [38] S. Kannan, *J. Mater. Sci.* **39** (2004) 6591–6600.
- [39] F. Rouquerol, J. Rouquerol, K. Sing, *Adsorption by Powders and Porous Solids*, Academic Press, Waltham, MA, 1999.
- [40] W.T. Reichle, S.Y. Kang, D.S. Everhardt, *J. Catal.* **101** (1986) 352–359.
- [41] J.A. Gursky, S.D. Blough, C. Luna, C. Gomez, A.N. Luevano, E.A. Gardner, *J. Am. Chem. Soc.* **128** (2006) 8376–8380.
- [42] M. Tu, J. Shen, Y. Chen, *J. Solid State Chem.* **128** (1997) 73–79.
- [43] O.D. Pavel, D. Tichit, I.-C. Marcu, *Appl. Clay Sci.* **61** (2012) 52–58.
- [44] F. Cavani, L. Maselli, D. Scagliarini, C. Flego, C. Perego, *Stud. Surf. Sci. Catal.* **155** (2005) 167–177.
- [45] H.A. Prescott, Z.-J. Li, E. Kemnitz, A. Trunschke, J. Deutsch, H. Lieske, A. Auoux, *J. Catal.* **234** (2005) 119–130.
- [46] H. Du, C.T. Williams, A.D. Ebner, J.A. Ritter, *Chem. Mater.* **22** (2010) 3519–3520.
- [47] J. Shen, M. Tu, C. Hu, *J. Solid State Chem.* **137** (1998) 295–301.
- [48] F. Prinetto, G. Ghiootti, R. Durand, D. Tichit, *J. Phys. Chem. B* **104** (2000) 11117–11126.
- [49] A.P. Grosvenor, B.A. Kobe, M.C. Biesinger, N.S. McIntyre, *Surf. Interface Anal.* **36** (2004) 1564–1570.
- [50] M. Descotes, F. Mercier, N. Thromat, C. Beaucaire, M. Gautier-Soyer, *Appl. Surf. Sci.* **165** (2000) 288–302.
- [51] M. Hadnadjev, T. Vulic, R. Marinkovic-Neducin, Y. Suchorski, H. Weiss, *Appl. Surf. Sci.* **254** (2008) 4297–4300.
- [52] R.J. Balasamy, A. Khurshid, A.A.S. Al-Ali, L.A. Atanda, K. Sagata, M. Asamoto, H. Yahiro, K. Nomura, T. Sano, K. Takehira, S.S. Al-Khattaf, *Appl. Catal., A* **390** (2010) 225–234.
- [53] T.L. Barr, *J. Phys. Chem.* **82** (1978) 1801–1810.
- [54] A.C. Heredia, M.I. Oliva, C.I. Zandalazini, U.A. Agú, G.A. Eimer, S.G. Casuscelli, E.R. Herrero, C.F. Pérez, M.E. Crivello, *Ind. Eng. Chem. Res.* **50** (2011) 6695–6700.
- [55] M. Richter, Y.K. Krisnandi, R. Eckelt, A. Martin, *Catal. Commun.* **9** (2008) 2112–2120.
- [56] B. De Meulenaer, B. Vanhoutte, A. Huyghebaert, *Chromatographia* **51** (2000) 44–52.
- [57] A. Martin, M.P. Checinski, M. Richter, *Catal. Commun.* **25** (2012) 130–135.
- [58] D. Tichit, M.H. Lhouty, A. Guida, B.H. Chiche, F. Figueras, A. Auoux, D. Bartalini, E. Garrone, *J. Catal.* **151** (1995) 50–59.